electronics

MDPI

Article

MPB-UNet: Multi-Parallel Blocks UNet for MRI Automated Brain Tumor Segmentation

Fatma Chahbar [1,2,*], Medjeded Merati [2,3] and Saïd Mahmoudi [4,*]

[1] Laboratoire de Génie Energétique et Génie Informatique (L2GEGI), University of Tiaret, Tiaret 14000, Algeria
[2] Department of Computer Science, University of Tiaret, Tiaret 14000, Algeria; medjeded.merati@univ-tiaret.dz
[3] Laboratoire d'Informatique et Mathematique (LIM), University of Tiaret, Tiaret 14000, Algeria
[4] Department of Computer Science, University of Mons, 7000 Mons, Belgium
* Correspondence: fatma.chahbar@univ-tiaret.dz or fatma.chahbar@gmail.com (F.C.); said.mahmoudi@umons.ac.be (S.M.); Tel.: +213-797971973 (F.C.)

Abstract: Brain tumor segmentation in Magnetic Resonance Imaging (MRI) is crucial for accurate diagnosis and treatment planning in neuro-oncology. This paper introduces a novel multi-parallel blocks UNet (MPB-UNet) architecture for automated brain tumor segmentation. Our approach enhances the standard UNet model by incorporating multiple parallel processing paths, inspired by the human visual system's multi-scale processing capabilities. We integrate Atrous Spatial Pyramid Pooling (ASPP) to effectively capture multi-scale contextual information. We evaluated our proposed architecture using the publicly available Low-Grade Glioma (LGG) Segmentation Dataset. This comprehensive collection comprises 3929 axial slices of FLAIR MRI sequences from 110 patients, each slice paired with a corresponding segmentation mask. Our model demonstrated superior performances on this dataset compared with existing state-of-the-art methods, highlighting its effectiveness in accurate tumor delineation. We provide a comprehensive analysis of the model's performance, including visual results and comparisons with other architectures. This work contributes to advancing automated brain tumor segmentation techniques, potentially improving diagnostic accuracy and efficiency in clinical settings. The proposed multi-parallel blocks UNet shows promise for integration into clinical workflows and opens avenues for future studies in medical image analysis. Our model achieves strong performances across multiple metrics: 99.86% accuracy, 99.86% precision, 99.86% sensitivity, 99.86% specificity, 99.80% Dice Similarity Coefficient (DSC), and 92.17% Average Intersection over Union (IoU).

Keywords: brain tumor segmentation; UNet; ASPP; semantic segmentation; cancer; brain tumor; MRI

Academic Editor: Michael Winter

Received: 2 November 2024
Revised: 17 December 2024
Accepted: 23 December 2024
Published: 26 December 2024

Citation: Chahbar, F.; Merati, M.; Mahmoudi, S. MPB-UNet: Multi-Parallel Blocks UNet for MRI Automated Brain Tumor Segmentation. *Electronics* **2025**, *14*, 40. https://doi.org/10.3390/electronics14010040

1. Introduction

The human brain is the central organ of the nervous system, crucial for controlling vital bodily functions and cognitive processes [1]. It receives and processes signals from various organs, interprets sensory information, and coordinates responses crucial for survival and daily activities [2]. The brain's complexity and importance make it a critical focus of medical research and diagnosis [3]. Given its pivotal role in human functionality, the presence of tumors in the brain can have profound and far-reaching consequences. Brain tumors can significantly disrupt normal neurological processes, potentially affecting everything from motor skills and sensory perception to cognitive functions and personality. The impact

of these tumors on brain activity can be severe, often leading to life-altering changes in a person's abilities and quality of life [4].

Tumors are abnormal cell masses that form in the body without serving any physiological function. They can be classified into two main categories: benign and malignant. Benign tumors are typically localized and non-invasive, often associated with more favorable prognoses. In contrast, malignant tumors, commonly known as cancerous tumors, have the capacity to invade surrounding tissues and metastasize to distant parts of the body [1]. While no organ is immune to tumor development, the occurrence of a tumor in the brain is particularly alarming due to its intricate structure and critical functions. Intracranial tumors manifest as unregulated cellular proliferations within or adjacent to brain tissue [5]. The origins of these cerebral neoplasms remain poorly understood, and their early detection is often hindered by a lack of clear initial symptoms. As a result, patients are frequently unaware of the severity of their condition until pronounced symptoms emerge or the tumor is incidentally discovered through imaging techniques [6].

Brain and central nervous system (CNS) cancers posed a substantial global health threat in 2023, resulting in an estimated 250,000 deaths worldwide [7]. These cancers are typically categorized as either metastatic or primary, with the latter originating within the brain itself. Among primary brain tumors, meningiomas are the most common, accounting for 35% of cases, followed by glioblastomas at 16% and pituitary tumors at 14% [8]. This diverse range of tumor types, each presenting its own set of challenges in diagnosis and treatment, contributes significantly to the overall burden of CNS cancers, solidifying their position as a major cause of cancer-related mortality worldwide.

Early diagnosis and treatment of tumors are essential in improving the prognosis and lifespan of patients. Various advanced medical imaging technologies enable detailed visualization of brain structures [9]. Advanced medical imaging techniques, including MRI, CT, and X-ray, are now fundamental to clinical diagnostics, providing intricate views of internal anatomy. Image segmentation has emerged as a critical process in this field, enabling the precise delineation of anatomical structures within these images. This powerful technique forms the cornerstone of accurate clinical diagnosis and early disease detection, substantially enhancing physicians' ability to identify and characterize abnormalities. By improving diagnostic precision, image segmentation plays a vital role in advancing patient care across a wide range of medical conditions. Radiologists primarily use structural MRI scans for diagnosing brain tumors, as they can provide detailed information on the cellular, functional, metabolic, and vascular features of the brain. The use of multimodality and multi-orientation MRI approaches has proven highly beneficial for analyzing complex brain tumor tissue [10]. This multimodal MRI technique combines several imaging sequences, including T1, T1-Gadolinium, T1-Weighted, T2, T2-W, and FLAIR, into a unified diagnosis. Each of these imaging types provides a unique perspective on brain architecture and potential pathologies, resulting in a more comprehensive diagnostic process [10].

The management of intracranial neoplasms necessitates a comprehensive, team-based strategy incorporating diagnostic imaging, systemic drug therapy, and surgical intervention within the central nervous system. Treatment decisions are based on multiple factors such as tumor grade, location, size, and type. Manual diagnosis of brain tumors presents significant challenges due to the complexity and variability of these factors. Analyzing numerous MRI slices across various orientations and modalities in a clinical setting is time-consuming and complex. Consequently, there is a pressing need for automated techniques in brain tumor classification and segmentation to enhance diagnostic accuracy and efficiency [11].

Convolutional Neural Networks (CNNs), a product of recent breakthroughs in machine learning and computer vision, have emerged as potent tools in medical imaging. These sophisticated models have proven to be highly effective in tackling complex

Computer-Aided Diagnosis (CAD) challenges [12]. CNNs excel in various tasks crucial for brain tumor analysis, including image recognition, tumor classification, precise segmentation, and early detection. Their ability to automatically learn and extract relevant features from medical images has significantly enhanced the accuracy and efficiency of diagnostic processes [13].

In this paper, we propose a novel multi-parallel blocks UNet architecture with integrated Atrous Spatial Pyramid Pooling (ASPP) [14] for brain tumor segmentation. Our approach builds upon the standard UNet model [15] to enhance shape recognition and improve segmentation accuracy. We evaluate our model on the Low-Grade Glioma (LGG) Segmentation Dataset, demonstrating superior performance compared with existing state-of-the-art methods. The main contributions of this work include the following:

- A novel multi-parallel blocks UNet architecture that enhances feature extraction through parallel processing paths, inspired by the multi-scale processing capabilities of the human visual system. This design enables comprehensive feature analysis at multiple levels, leading to more robust tumor boundary detection and improved segmentation accuracy.
- Integration of Atrous Spatial Pyramid Pooling (ASPP) to enhance multi-scale feature extraction. ASPP utilizes parallel atrous convolutions with varying dilation rates, enabling the simultaneous processing of features at multiple scales. This approach improves segmentation accuracy for brain tumors of diverse sizes and shapes in MRI images.

Through this work, we aim to advance the field of automated brain tumor segmentation, potentially improving diagnostic accuracy and efficiency in clinical settings.

This paper is organized as follows: Section 2 provides an overview of related work in brain tumor segmentation. Section 3 describes our proposed methodology, the multi-parallel blocks UNet architecture and its components. Section 4 presents the experimental results, dataset description, evaluation metrics, and comparative analysis with other methods. Finally, Section 5 concludes the paper and discusses potential future directions for this research.

2. Related Work

Several works have applied deep learning techniques to the segmentation, detection, and classification of brain tumors in MRI images. For instance, hybrid CNNs that follow a patch-based approach can be used in this application to enable the network to merge contextual and local information. Table 1 shows the segmentation and classification architectures proposed by different authors for brain tumors, with their results compared using the Dice Similarity Coefficient (DSC) or accuracy measures.

Francisco Javier et al. [16] proposed a fully automatic model for segmenting and classifying brain tumors using a Deep CNN multiscale approach. This method processes input images at three spatial scales along different processing pathways, which are concatenated to provide output for four different classes using a fully connected layer. The use of elastic transformation helps prevent overfitting by serving as a data augmentation procedure.

The proposed hybrid CNN architecture by Sajid et al. [17] adopted a patchwise approach for output label prediction. They used batch normalizations with dropouts as regularizers to tackle the problem of overfitting. In this study, preprocessing was performed through normalization and bias field correction.

Farajzadeh Nacer et al. [18] proposed an integrated hybrid approach combining deep CNN and machine learning classifiers to accurately segment and classify brain MRI tumors. In the first stage, a CNN is used to learn the feature map of the brain MRI image, identifying marker regions within the tumor. In the second phase, a faster region-based Convolutional

Neural Network (FR-CNN) is designed to localize the tumor region followed by a Region Proposal Network (RPN). Finally, in the last stage, deep CNN and SVM-RBF classifiers are built in series to further refine the segmentation and classification, resulting in more accurate findings.

Sangeeta Kakarwal and Rahul Mapari [19] developed an automatic brain tumor segmentation and detection system using a dense CNN. Their approach aimed to segment tumor regions in MRI scans by employing approximate c-means clustering and improve brain disease classification accuracy using a Black Widow Optimization-Driven Dense CNN (BW-DCNN). The process also included preprocessing techniques such as Gaussian filtering and Contrast Limited Adaptive Histogram Equalization (CLAHE).

Sergio Pereira et al. [20] proposed a hierarchical system for whole tumor segmentation and intratumoral tissue segmentation. They utilized histogram standardization as a preprocessing technique and implemented a fully CNN-based UNet architecture. The non-linear activation function used in their model was the Leaky Rectified Linear Unit (Leaky ReLU).

Archana Ingle et al. [21] introduced a fully automated brain tumor segmentation and classification model based on an encoder–decoder architecture, which enhances on the existing UNet design with ResNet embedding. The model's performance was further improved by implementing several augmentation approaches.

In another study, Mohamed Naser et al. [22] adopted a deep learning approach by combining Convolutional Neural Networks for segmenting tumors using UNet and pretrained VGG16 convolutions with transfer learning, paired with a fully connected classifier for grading the tumor. The dataset was augmented using rotation, zoom, shift, and horizontal flip operations.

Sujatha et al. [23] introduced a CNN algorithm utilizing a VGG16 pretrained model for detecting brain tumors in MRI images. The input images undergo segmentation using a UNet model to enhance prediction accuracy and are subsequently classified with the VGG16-based CNN for efficient and rapid detection. Preprocessing involves converting color images to grayscale, normalizing them, and enhancing contrast using CLAHE.

Dan Xu et al. [24] developed an automatic segmentation algorithm for low-grade glioma in MRI images based on the UNet++ model. The input MRI images undergo preprocessing, including normalization to standardize the data and reduce lighting inconsistencies. Data augmentation techniques such as flipping, rotation, and translation are applied to increase the training sample size and improve model generalization. The preprocessed and augmented images are then fed into the UNet++ architecture, which utilizes dense skip connections to enhance feature fusion between the encoder and decoder paths.

Punam Bedi et al. [25] proposed a novel hybrid model named "CT-γ-Net" for effective and efficient brain tumor localization. This model integrates a Convolutional Encoder and a Transformer Encoder for encoding and a Convolutional Decoder for decoding the combined output to generate segmentation masks. By utilizing Depth-Wise Separable convolutional layers, the model significantly reduces the number of trainable weight parameters.

Anila Kunjumon et al. [26] proposed a hybrid U-Net model with a ResNet50 encoder for segmenting low-grade gliomas in MRI brain images. The preprocessing involved resizing images to 256 $\times$ 256 pixels and handling missing sequences. The approach surpassed existing methods in LGG segmentation, demonstrating effective tumor region identification. The ResNet50 encoder helped address vanishing gradients, while the U-Net decoder enabled precise segmentation.

While these studies show significant advancements in brain tumor segmentation using deep learning, challenges remain in achieving high accuracy for complex tumor structures and effectively capturing multi-scale features. Our work aims to address these limitations through a novel architecture that enhances feature extraction and segmentation accuracy.

Table 1. Overview of related work on brain tumor segmentation and classification.

Author	CNN Architecture	Dataset	Performance
Francisco Javier et al. (2021) [16]	Three-path output concatenation CNN	Nanfang Hospital	DSC: 82.8%
Sajid et al. (2019) [17]	hybrid architecture of CNN	BraTS 2013	DSC: 86%
Farajzadeh Nacer et al. (2023) [18]	Deep CNN+ SVM-RBF	Figshare dataset	Accuracy: 98%
Sangeeta Kakarwal and Rahul Mapari. (2024) [19]	BW-DCNN	Private data	Accuracy: 92%
Sergio Pereira et al. (2016) [20]	Fully CNN-based UNet	BraTS 2013	DSC: 85%
Archana Ingle et al. (2022) [21]	ResUNet2	Nanfang Hospital	DSC: 83.69%
Mohamed Naser et al. (2020) [22]	UNet	LGG dataset (Kaggle)	DSC: 84%
Sujatha et al. (2024) [23]	UNet	LGG dataset (Kaggle)	DSC: 90%
Dan Xu et al. (2020) [24]	UNet++	LGG dataset (Kaggle)	DSC: 89.1%
Punam Bedi et al. (2024) [25]	CT-γ-Net	LGG dataset (Kaggle)	Accuracy: 99.24%
Anila Kunjumon et al. (2024) [26]	An efficient U-Net	LGG dataset (Kaggle)	Accuracy: 99.8%, DSC: 82%

3. Methodology

In our methodology, brain MRI images first undergo analysis through a classification module that determines whether a tumor is present and, if so, identifies its specific type. This classification phase utilizes an advanced approach developed by Chahbar et al. [27], which combines Convolutional Neural Networks (CNNs) with transfer learning techniques from both VGG19 and ResNet architectures to maximize classification accuracy. The model distinguishes between four distinct categories: No Tumor, Meningioma, Glioma, and Pituitary, achieving a remarkable accuracy rate of 98.26%. Following classification, the images are then processed through a segmentation module, which serves as a secondary verification system to validate the initial classification decision and provide an additional layer of confirmation through detailed image analysis. This segmentation module, based on an enhanced UNet model, accurately delineates the tumor regions within the MRI images. The final output offers a clear visualization of the tumor's location and boundaries with an identification of tumor type with percentages; this percentage is based on the classification result. This global architecture effectively integrates classification and segmentation, facilitating accurate diagnosis and treatment planning for brain tumor cases, as illustrated in Figure 1.

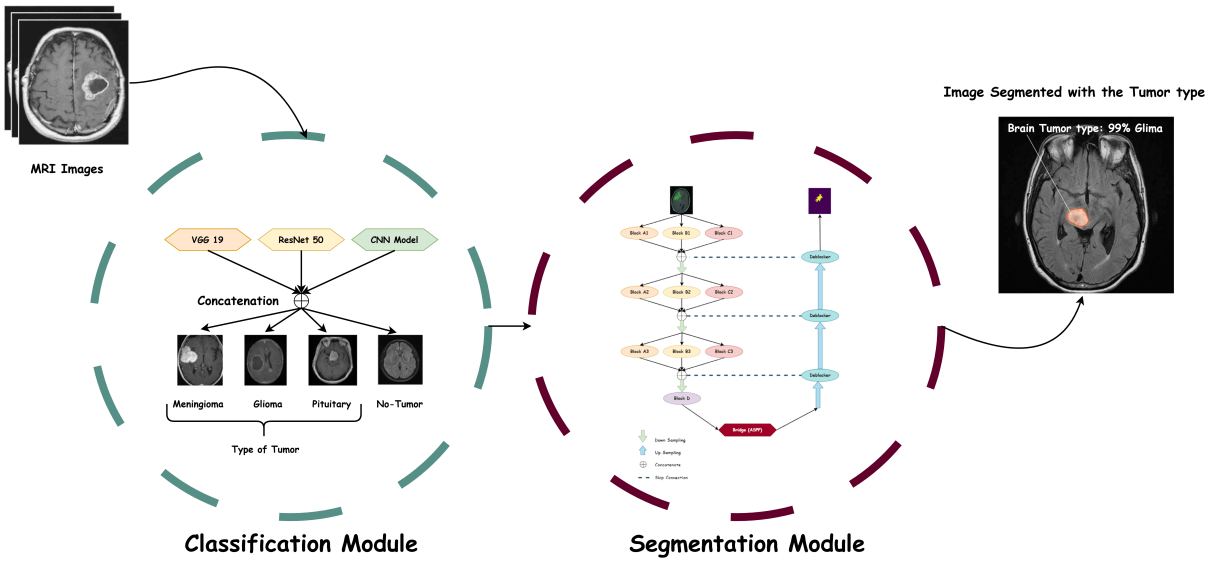

Figure 1. Global architecture for brain tumor classification and segmentation.

3.1. Segmentation Module

Image segmentation in medical imaging is crucial for identifying and analyzing anatomical structures, particularly in brain tumor analysis where precise delineation of

tumor boundaries is essential for diagnosis and treatment planning. While a traditional UNet architecture has been effective for medical image segmentation, we propose an enhanced multi-parallel blocks UNet (MPB-UNet) that introduces parallel processing paths and ASPP for improved feature extraction and segmentation accuracy.

3.1.1. UNet

UNet is a CNN model designed specifically for semantic segmentation [15]. It features a symmetric structure composed of two main components: an Encoder and a Decoder. The Encoder extracts spatial features from the input image, following a standard convolutional network format. Each stage in the Encoder consists of two 3×3 convolutional layers, followed by a 2×2 max-pooling operation with a stride of 2, and this sequence is repeated four times. With each downsampling step, the number of filters in the convolutional layers doubles. The transition from the Encoder to the Decoder is facilitated by a series of two 3×3 convolutional layers [28].

On the other hand, the Decoder reconstructs the segmentation map by upsampling the feature maps. This process starts with a 2×2 transposed convolution operation, which halves the number of feature channels, followed by two 3×3 convolution operations. This upsampling and convolution sequence is repeated four times, with the number of filters halving at each step. The final segmentation map is produced by a 1×1 convolution layer. Except for the final layer, which employs a sigmoid activation function, all convolutional layers utilize the ReLU (Rectified Linear Unit) activation function [28].

A unique feature of the UNet architecture is the inclusion of skip connections. At each of the four levels, the feature maps from the convolutional layer before pooling in the Encoder are transferred to the Decoder. These maps are concatenated with the output from the upsampling operation and passed through subsequent layers. Skip connections help recover spatial information that may be lost during pooling operations [28]. The overall architecture is visually depicted in Figure 2.

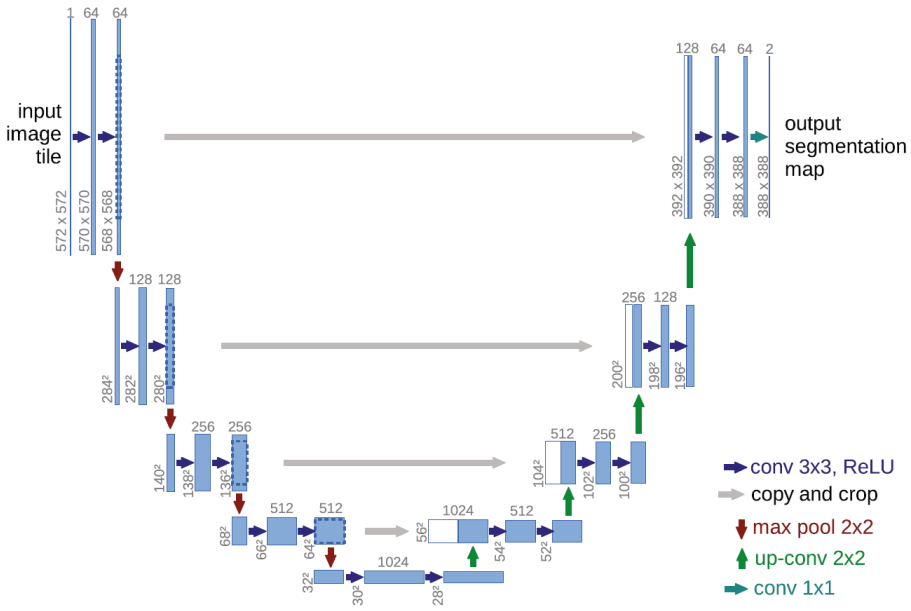

Figure 2. UNet architecture [15].

3.1.2. MPB-UNet Architecture

The novel architecture illustrated in Figures 3 and 4 is inspired by the inherent operation of the human visual system (HVS) and builds upon the classical UNet architecture. This design aims to enhance feature extraction and segmentation performance through a

combination of specialized blocks and skip connections. The architecture flow, depicted in Figure 3, starts with the input image being processed through three parallel paths utilizing Block A1, Block B1, and Block C1. One key difference between our proposed model and previous works is that input images are processed at three spatial scales along different processing pathways, a mechanism inspired by the operation of the HVS. The parallel processing mechanism allows the network to simultaneously extract features at different abstraction levels, similar to how the HVS processes visual information at multiple scales concurrently. The outputs from these initial blocks are concatenated; this concatenated output is then downsampled using max-pooling operations to reduce spatial dimensions while preserving the most important features, and then passed through the next set of blocks (A2, B2, C2) for further feature extraction. This process continues until reaching Block D, which connects to the ASPP Bridge.

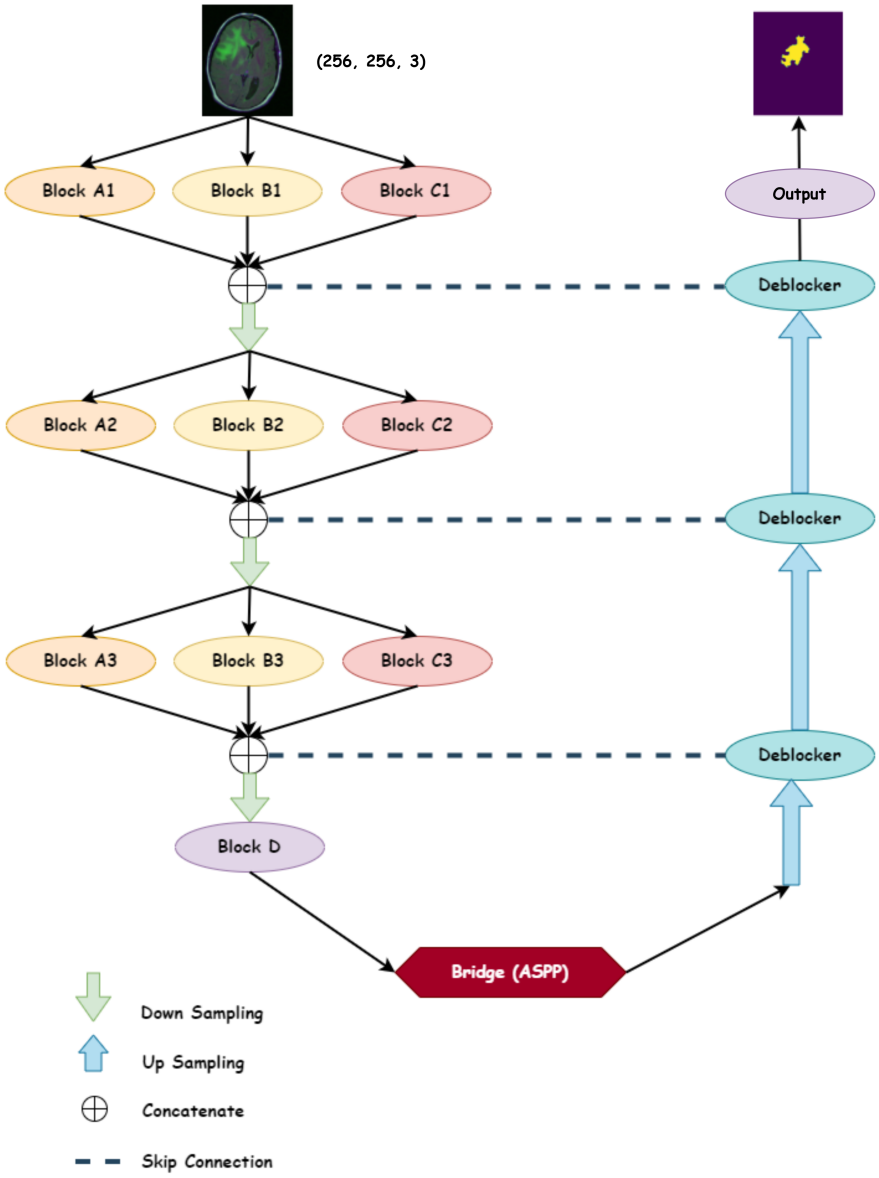

Figure 3. Multi-parallel blocks UNet architecture.

The ASPP Bridge incorporates parallel dilated convolutions with rates of (6, 12, 18), enabling the network to capture multi-scale contextual information without losing resolu-

tion. This design choice is particularly crucial for brain tumor segmentation, where features exist at various scales and maintaining spatial relationships is essential.

During the upsampling phase, features are processed through Deblocker modules that integrate skip connections from the corresponding downsampling stages to retain spatial information. The final output is a precise segmentation map reconstructed from the upsampled features. By mimicking the multi-scale processing capabilities of the HVS, this proposed architecture significantly enhances the performance of UNet in semantic segmentation tasks.

As shown in Figure 4, the architecture consists of several unique blocks: Block A, which features two 3×3 convolutional layers followed by Batch Normalization, ReLU activation, and a 20% dropout layer; Block B, with a single 3×3 convolutional layer, Batch Normalization, and ReLU activation; Block C, mirroring Block B's structure; and Block D, which comprises a single 3×3 convolution layer, Batch Normalization, and ReLU activation. Additionally, the Deblocker module consists of two sets of 3×3 convolution layers, each followed by Batch Normalization and ReLU activation, concluding with a concatenation operation. For the output layer, we have a 1×1 2D convolution layer and sigmoid activation function for the binary classification of pixels.

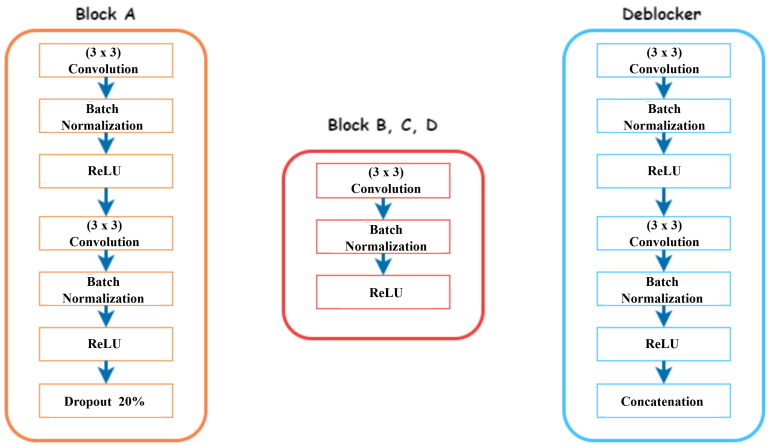

Figure 4. Definition of blocks.

The number of filters in each block plays a crucial role in the network's ability to effectively extract and process features. Table 2 provides a detailed breakdown of the filter counts used in each block of our MPB-UNet architecture. As we move deeper into the network, the number of filters increases, allowing for the extraction of more complex features. This progressive increase, combined with multi-path processing and skip connections, enables our architecture to capture a rich hierarchy of features at different scales.

Table 2. Filter configuration in multi-parallel blocks UNet architecture.

Block	Number of Filters
A1	16
B1	16
C1	32
A2	32
B2	32
C2	64
A3	64
B3	64
C3	128
D	1024
Deblockers	512, 256, 128

3.1.3. Atrous Spatial Pyramid Pooling

Atrous Spatial Pyramid Pooling (ASPP) is a powerful technique introduced by Chen et al. in their DeepLab series of papers [14]. ASPP is designed to capture multi-scale context information effectively, which is crucial for accurate semantic segmentation, especially in tasks like brain tumor segmentation where the size and shape of the target regions can vary significantly.

The key idea behind ASPP is the use of atrous (or dilated) convolutions at multiple rates. Atrous convolutions allow the network to expand the field of view without increasing the number of parameters or the amount of computation [29]. By applying multiple atrous convolutions with different dilation rates in parallel, ASPP can capture features at multiple scales simultaneously.

The structure of ASPP typically includes a 1×1 convolution, several 3×3 convolutions with different atrous rates (e.g., rates of 6, 12, and 18), and a global average pooling operation. These parallel operations are then concatenated and passed through a final 1×1 convolution to produce the output feature map, as shown in Figure 5.

The effectiveness of ASPP has been demonstrated in various segmentation tasks. For instance, in the DeepLabv3+ architecture [30], ASPP was shown to significantly improve performance on the PASCAL VOC 2012 and Cityscapes datasets. In medical image segmentation, ASPP has been successfully applied to tasks such as liver segmentation [31] and breast ultrasound lesion segmentation [32]. In the context of brain tumor segmentation, ASPP can be particularly beneficial. Brain tumors can vary greatly in size, shape, and location, and capturing this variability requires processing at multiple scales. By incorporating ASPP into our MPB-UNet architecture, we enhance the model's ability to capture precise details of tumor boundaries while also maintaining awareness of the broader context within the brain MRI. It is worth noting that while ASPP is powerful, it does come with increased computational cost. Some researchers have proposed modifications to improve efficiency. For example, Chen et al. [33] introduced a "Dense ASPP" variant that uses densely connected atrous convolutions to further improve multi-scale feature extraction while reducing the number of parameters.

In our implementation, we incorporate the standard ASPP architecture between the encoder and decoder sections of our MPB-UNet, allowing it to refine the multi-scale features extracted by the encoder before they are processed by the decoder for final segmentation.

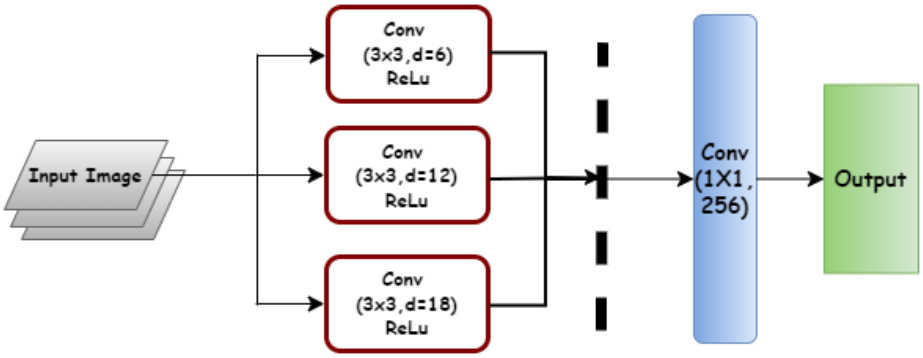

Figure 5. Network architecture with integrated spatial pyramid pooling for multi-scale feature extraction.

4. Results and Discussion

This section provides a comprehensive analysis of our proposed MPB- UNet architecture for brain tumor segmentation. We begin by describing the experimental dataset used for training and evaluating our model. Next, we outline the evaluation metrics employed to assess the model's performance. Finally, we present our results and compare them with

existing state-of-the-art methods in brain tumor segmentation. Through this discussion, we aim to demonstrate the effectiveness and potential advantages of our proposed architecture in accurately delineating brain tumor regions from MRI images.

4.1. Experimental Dataset

For our experiments, we utilized the Low-Grade Glioma (LGG) Segmentation Dataset, a publicly available collection of brain MRI images with corresponding segmentation masks [34]. Compiled by Mateusz Buda and hosted on Kaggle, this dataset consists of MRI scans from 110 patients diagnosed with LGG. It includes 3929 axial slices of FLAIR (Fluid Attenuated Inversion Recovery) MRI sequences, each accompanied by a manual segmentation mask delineating the FLAIR abnormality. FLAIR sequences are particularly effective in highlighting brain abnormalities, especially in white matter regions.

The original images have dimensions of 256 × 256 pixels and are provided in .tif format with three channels, corresponding to pre-contrast, FLAIR, and post-contrast sequences [34]. To prepare and optimize our dataset, we performed the following:

1. Split the dataset into training, validation, and test sets, with 80% of the data used for training and validation and 20% for testing. This division ensures a robust evaluation of our model's performance.
2. Implemented comprehensive data augmentation techniques during the training phase, including random rotation (20 degrees), horizontal and vertical flips, random brightness adjustments (5%), random contrast variations (5%), and random cropping. These augmentation strategies were carefully selected to reflect realistic variations in medical imaging while preserving the critical diagnostic features of the brain images.

During the training process, we used a buffer size of 1000 and a batch size of 32 to efficiently manage memory usage and optimize training speed. This resized and partitioned dataset retains the original characteristics, including the notable class imbalance typical in medical imaging tasks, where tumor regions often occupy only a small portion of the entire brain volume. This aspect makes the LGG Segmentation Dataset particularly valuable for evaluating the robustness and accuracy of segmentation models in realistic medical imaging scenarios. The dataset's combination of high-quality FLAIR images, precise manual segmentations, and representation of various tumor shapes and sizes provides an excellent foundation for training and testing our proposed segmentation algorithm. Figure 6 illustrates examples from the dataset, highlighting both the images and the annotated masks.

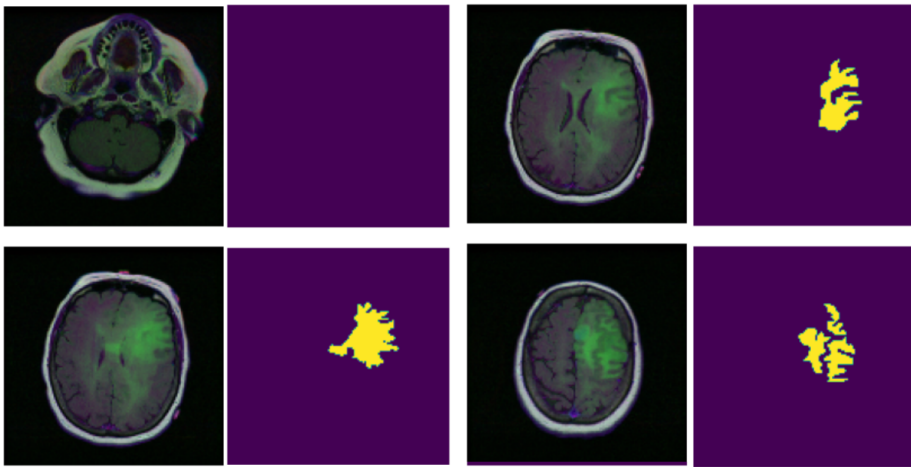

Figure 6. Examples of images and their corresponding masks from the LGG Dataset [34].

4.2. Evaluation Metrics

The performance of our model was assessed using several quantitative measures commonly used to evaluate performance in medical image segmentation tasks. These metrics provide a detailed assessment of segmentation accuracy and efficiency. For each metric, higher scores indicate better segmentation performance. The evaluation criteria are defined by accuracy, intersection over union (IoU), Dice score, sensitivity, specificity, and precision, which are mathematically expressed as follows:

$$\text{Accuracy} = \frac{\text{TP} + \text{TN}}{\text{TP} + \text{TN} + \text{FN} + \text{FP}} \tag{1}$$

$$\text{IoU} = \frac{\text{TP}}{\text{TP} + \text{FP} + \text{FN}} \tag{2}$$

$$\text{Dice score} = \frac{2\text{TP}}{2\text{TP} + \text{FN} + \text{FP}} \tag{3}$$

$$\text{Specificity} = \frac{\text{TN}}{\text{TN} + \text{FP}} \tag{4}$$

$$\text{Sensitivity} = \frac{\text{TP}}{\text{TP} + \text{FN}} \tag{5}$$

$$\text{Precision} = \frac{\text{TP}}{\text{TP} + \text{FP}} \tag{6}$$

- True positive (TP) represents the correctly identified tumor areas, where the predicted tumor region matches the actual tumor region in the ground truth.
- True negative (TN) indicates the correctly identified non-tumor areas, where both the prediction and the ground truth agree on the absence of a tumor.
- False positive (FP) occurs when the model incorrectly predicts a tumor in an area where no actual tumor is present.
- False negative (FN) represents instances where the model fails to detect an actual tumor, misclassifying it as non-tumor tissue.

4.3. Discussions and Comparisons

Our proposed MPB-UNet architecture was implemented and evaluated using the Kaggle open-source platform, leveraging its robust computational resources. The experimental environment was meticulously configured with a comprehensive hardware and software setup. The experimental environment consisted of a CPU with four cores and 30 GB of RAM, complemented by an NVIDIA Tesla P100 GPU with 13 GB of RAM. In our experiments, we specifically utilized NVIDIA Tesla T4 GPUs, each equipped with 13 GB of RAM, to enable parallel tensor processing and enhance computational efficiency. This high-performance setup enabled us to efficiently train and test our model, providing a robust platform for comprehensive model exploration and validation. In the following sections, we present a detailed analysis of the results obtained from our experiments.

4.3.1. Training Phase Analysis

To demonstrate the efficacy of our proposed MPB-UNet architecture, we conducted a comparative analysis against several model variants and the classical UNet. This comparison aims to highlight the impact of different architectural components on segmentation performance. The models included in the comparison are as follows:

- Model 01: Incorporates Blocks A1, B1, and C1 in the encoder, with a single decoder block in the decoder path.The model has a total of 190,290 parameters (743.32 KB), of which 189,618 (740.70 KB) are trainable and 672 (2.62 KB) are non-trainable parameters.
- Model 02: Expands on Model 01 by including Blocks A2, B2, and C2, along with a concatenation operation in the encoder, while retaining two decoder blocks in the decoder path. The model has a total of 3,617,594 parameters (13.80 MB), of which 3,615,306 (13.79 MB) are trainable and 2288 (8.94 KB) are non-trainable parameters.
- Model MPB-UNet (Model 03): Incorporates three stages in the encoder (from A1, B1, C1 to A3, B3, C3) as represented in Figure 3, with three corresponding decoder blocks and skip connections.The model has a total of 12,167,474 parameters (46.42 MB), of which 12,162,514 (46.40 MB) are trainable and 4960 (19.38 KB) are non-trainable parameters.
- Model 04: Represents our full proposed architecture, encompassing all blocks from A1 to A4 (and corresponding B and C blocks) in the encoder, coupled with four Deblocker modules in the decoder. The model has a total of 21,170,610 parameters (80.76 MB), of which 21,162,322 (80.73 MB) are trainable and 8288 (32.38 KB) are non-trainable parameters.
- Classical UNet: A baseline model implementing the standard U-Net architecture with four levels.The model has a total of 5,027,010 parameters (19.18 MB), of which 5,022,402 (19.16 MB) are trainable and 4608 (18.00 KB) are non-trainable parameters.

To thoroughly evaluate our proposed multi-parallel blocks UNet, its variants, and the classical UNet, we employed a comprehensive approach combining quantitative metrics with a visual analysis of the training dynamics. This evaluation provides valuable insights into the incremental improvements achieved through our architectural enhancements.

We assessed the performance of each model using a robust set of metrics widely used in medical image segmentation tasks: accuracy, precision, sensitivity (also known as recall), specificity, and DSC.

Our analysis demonstrates the effectiveness of the proposed MPB-UNet for brain tumor segmentation tasks. Each model was trained using a carefully designed optimization strategy with key parameters including a binary cross-entropy loss function well suited for binary segmentation tasks, a batch size of 32 balancing computational efficiency and gradient stability, 45 epochs ensuring sufficient model convergence while mitigating overfitting risks, and the Adam optimization algorithm with a learning rate of 0.001, leveraging adaptive moment estimation for efficient parameter updates.

By thoroughly evaluating performance across multiple quantitative metrics and analyzing training dynamics, we highlight the model's strengths in various aspects of segmentation quality. Table 3 presents the quantitative results of our evaluation, showcasing the performance of each model across different metrics. This detailed assessment reveals the advantages of our architectural enhancements and their significant impact on model performance, further validating the efficacy of the MPB-UNet approach.

Table 3. Training performance comparison of different model architectures.

Model	Accuracy (%)	Precision (%)	Sensitivity (%)	Specificity (%)	DSC (%)	Loss	Computing Time (Min)
Classical UNet	99.73	99.73	99.73	99.73	99.64	0.0059	63.16
Model 01	99.39	99.39	99.39	99.39	98.99	0.022	22.32
Model 02	99.81	99.81	99.81	99.81	99.72	0.01	30.75
Model 04	99.75	99.75	99.75	99.75	99.69	0.01	83.99
MPB-UNet	99.86	99.86	99.86	99.86	99.80	0.0033	66.59

As shown in Table 3, our proposed MPB-UNet demonstrates superior performance across all metrics, achieving the highest accuracy scores (up to 99.86%) and the lowest loss (0.0033), consistently outperforming simpler models. The training time increased proportionally with model complexity, showing a progressive increment from Model 01 to Model 04 (ranging from 22.32 to 83.99 min) due to the additional computational requirements of deeper architectures. These quantitative results, along with the analysis of training dynamics, provide strong evidence for the effectiveness of our architectural enhancements. The incremental improvements over previous models highlight the UNet's capability to leverage its multi-parallel structure to capture complex data relationships.

4.3.2. Testing Phase Analysis

To further validate the performance of our models, we conducted a comprehensive testing phase using a separate test set of MRI images. This phase allows us to assess the generalization capabilities of each model and provides visual evidence of their segmentation accuracy. Table 4 presents a quantitative comparison of these models' performance, offering detailed insights into their segmentation capabilities through key metrics, including accuracy, precision, specificity, sensitivity, DSC, and loss, covering Classical UNet, Model 01, Model 02, Model 04, and multi-parallel blocks (MPB-UNet).

Table 4. Testing performance comparison of different model architectures.

Model	Accuracy (%)	Precision (%)	Sensitivity (%)	Specificity (%)	DSC (%)	Loss
Classical UNet	99.53	99.53	99.53	99.53	99.41	0.012
Model 01	99.14	99.14	99.14	99.14	98.63	0.026
Model 02	99.67	99.67	99.67	99.67	99.58	0.011
Model 04	99.71	99.71	99.71	99.71	99.62	0.01
MPB-UNet	99.82	99.82	99.82	99.82	99.74	0.004

The performance evaluation reveals remarkable segmentation capabilities across U-Net model architectures, with all variants achieving accuracy exceeding 99%. The multi-parallel blocks U-Net (MPB-UNet) leads with 99.82% accuracy, 99.74% DSC, and a minimal 0.004 loss, indicating superior tumor segmentation precision with significant improvements over all the architectures.

The observed results strongly support that our model achieves genuine learning rather than memorization, as evidenced by the consistent performance across training and testing sets. The model achieves 99.86% training accuracy and 99.82% testing accuracy, showing a minimal gap of 0.04%. Similarly, the Dice Similarity Coefficient (DSC) demonstrates robust generalization with 99.80% for training and 99.74% for testing, representing only a 0.06% difference. These marginal differences between training and testing performance, combined with our regularization strategies, indicate that the model has learned generalizable features rather than overfitting to the training data.

Figure 7 showcases sample results from our testing phase, displaying the original MRI image, the ground truth segmentation, and the predictions from each of the models (Classical UNet, Model 01, Model 02, Model 04, and multi-parallel blocks (MPB-UNet)).

As shown in the visual results, our MPB-UNet demonstrates superior segmentation accuracy, closely aligning with the ground truth masks. The incremental improvements from the Classical UNet to the final MPB-UNet are visually apparent, with each model showing progressively better delineation of tumor boundaries. In the case of extremely small tumors as shown in the last sample, all models, including the MPB-UNet, demonstrate segmentation limitations. The minimal tumor size presents challenges due to low contrast and limited distinguishable features. Even our proposed MPB-UNet struggles to

accurately capture the entire tumor boundary, highlighting the complexity of detecting microscopic lesions.

To evaluate our models' performance, we conducted comprehensive testing on a substantial dataset comprising 800 test images, organized into 25 batches with 32 images per batch. We used two key metrics for quantitative assessment: the Intersection over Union (IoU) and Dice Similarity Coefficient (DSC), computing the average scores across all test images. The results of this evaluation are presented in Table 5.

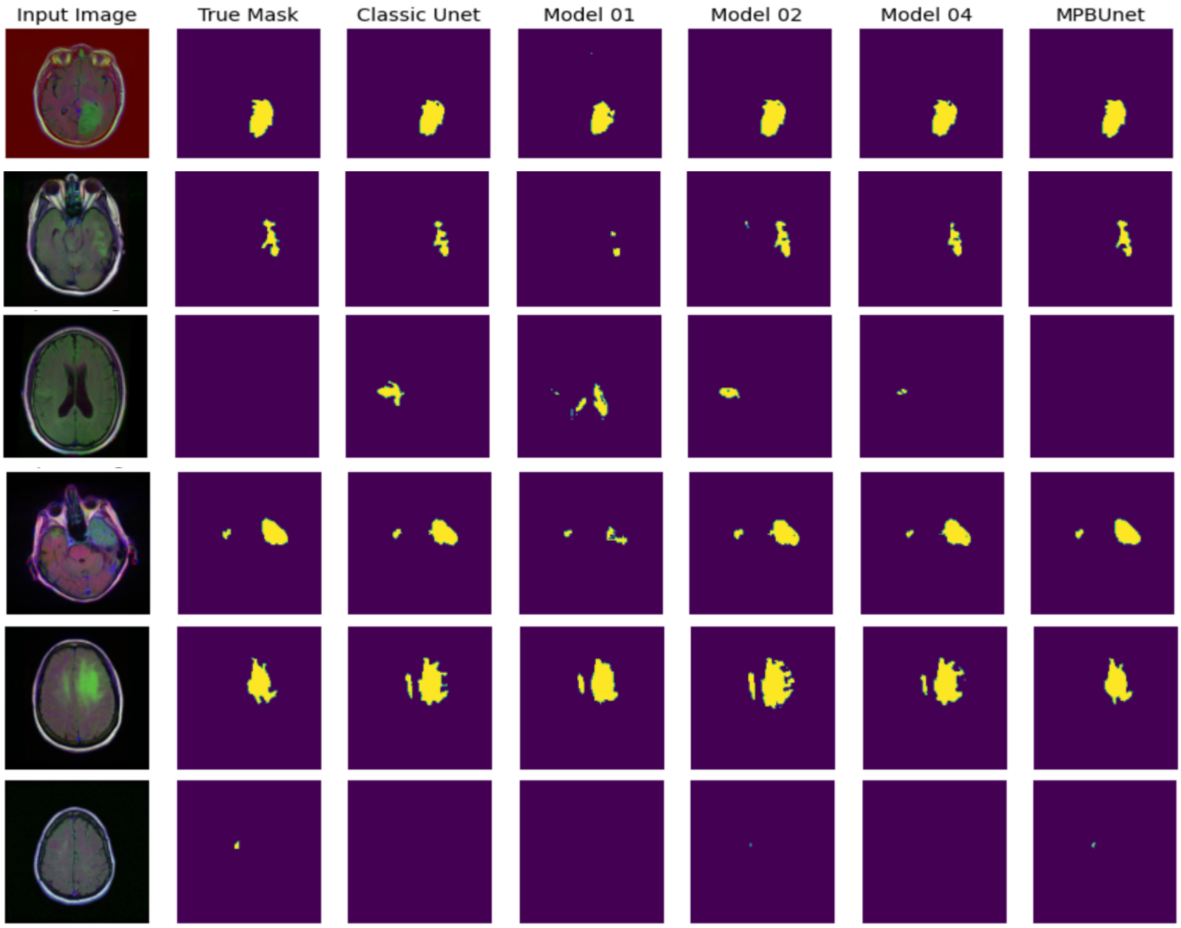

Figure 7. Sample segmentation results on test data. From left to right: original MRI image, ground truth, Classical UNet, Model 01, Model 02, Model 04, and MPB-UNet.

Table 5. Average IoU and DSC scores on the test set.

Model	Average IoU (%)	Average DSC (%)
Classical UNet	82.44	85.44
Model 01	58.42	61.86
Model 02	84.37	87.05
Model 04	87.40	90.14
MPB-UNet	92.17	94.43

The MPB-UNet achieves the highest average IoU of 92.17% and a DSC of 94.43%, outperforming the other models and demonstrating its superior segmentation capability. These results align with our earlier findings from the validation set and further solidify the effectiveness of our proposed architecture. The effectiveness of our MPB-UNet in accurately segmenting tumor regions is substantiated through rigorous statistical analysis using confusion matrices. Figure 8 illustrates the confusion matrices for the models: Classic

UNet, Model 01, Model 02, Model 04, and the MPB-UNet, each of which was evaluated on randomly selected brain tumor images. These matrices provide a comprehensive view of each model's performance in classifying tumor and non-tumor pixels. Notably, the MPB-UNet demonstrates superior performance, evidenced by a higher concentration of true positives (top-left quadrant) and true negatives (bottom-right quadrant) compared with the other models. This improvement is particularly evident when compared with Model 01, which exhibits a higher rate of misclassifications. The progressive improvement in classification accuracy from Model 01 to the MPB-UNet aligns with our earlier quantitative findings, further validating the effectiveness of our proposed architecture. These confusion matrices provide valuable insights into each model's sensitivity and specificity, crucial metrics in medical image analysis, and underscore the MPB-UNet's potential for reliable tumor detection in clinical applications.

Figure 8. Confusion matrices of the models (Classical UNet, Model 01, Model 02, Model 04, and MPB-UNet).

4.3.3. Analysis of MPB-UNet Performance

Among the evaluated models, the MPB-UNet consistently demonstrated superior performance in both the training and testing phases. This exceptional performance can be attributed to the following several key factors:

1. Optimal Architecture Depth: The MPB-UNet, with its three encoder and decoder stages, strikes an ideal balance between model complexity and feature extraction capability. Unlike shallower models, which may struggle to capture complex features, or deeper models, which might be prone to overfitting, the MPB-UNet achieves the optimal depth for this task.
2. Efficient Feature Extraction: The multi-parallel block structure in the MPB-UNet allows for the efficient extraction of features at multiple scales. This is particularly beneficial for brain tumor segmentation, where tumors can vary significantly in size and shape.
3. Reduced Overfitting: Compared with more complex models, the MPB-UNet has fewer parameters, which helps in reducing overfitting, especially given the limited size of

most medical imaging datasets. This is evidenced by its consistent performance across both training and test sets.

These factors combine to make the MPB-UNet particularly well suited for brain tumor segmentation, as demonstrated by its superior performance metrics during both the training and testing phases.

4.3.4. Comparative Analysis

To contextualize our MPB-UNet's performance, we compared recent brain tumor segmentation methods using the Low-Grade Glioma (LGG) Kaggle dataset, as summarized in Table 6. Mohamed Naser et al. (2020) [22] employed a UNet approach, achieving a Dice Similarity Coefficient (DSC) of 84%. Sujatha et al. (2024) [23] further advanced UNet techniques, reporting a DSC of 90%. Dan Xu et al. (2020) [24] introduced UNet++, demonstrating a DSC of 89.1%. Punam Bedi et al. (2024) [25] proposed the CT-γ-Net, reaching an impressive accuracy of 99.24%. Anila Kunjumon et al. (2024) [26] developed an Efficient U-Net, achieving 99.8% accuracy and an 82% DSC. These studies highlight the ongoing advancements in brain tumor segmentation techniques using deep learning architectures.

Our MPB-UNet demonstrates superior performance, achieving a Dice Similarity Coefficient (DSC) of 94.43% and an accuracy of 99.86% on the LGG Segmentation Dataset. These results significantly surpass most existing methods, including those using similar architectural foundations such as UNet variants. The marked improvement in both DSC score and accuracy highlights the effectiveness of our multi-parallel block design in capturing complex tumor features and boundaries. Notably, while some studies report only accuracy or DSC, our model excels in both, offering a more comprehensive evaluation of segmentation quality, particularly within the context of imbalanced datasets typical in medical imaging tasks.

Table 6. Comparison of our MPB-UNet with related state-of-the-art methods.

Author	DSC	Accuracy
Mohamed Naser et al. (2020) [22]	84%	–
Sujatha et al. (2024) [23]	90%	–
Dan Xu et al. (2020) [24]	89.1%	–
Punam Bedi et al. (2024) [25]	–	99.24%
Anila Kunjumon et al. (2024) [26]	82%	99.8%
Our work	99.80%	99.86%

5. Conclusions

This paper introduces a novel multi-parallel blocks UNet architecture for brain tumor segmentation in MRI images. Our model achieved superior performance on the LGG Segmentation Dataset, with a Dice Similarity Coefficient of 99.80% and an accuracy of 99.86%. The key innovations of our approach include multiple parallel processing paths inspired by the human visual system, the integration of Atrous Spatial Pyramid Pooling (ASPP), and a comprehensive evaluation framework across various metrics.

Our MPB-UNet architecture represents a significant advancement in automated brain tumor segmentation, with the potential to support clinical decision making in neuro-oncology. These results demonstrate the effectiveness of our approach in enhancing brain tumor segmentation accuracy. As deep learning continues to evolve, such approaches are likely to play an increasingly important role in improving patient outcomes in the field of neuro-oncology.

To further advance this research, we propose evaluating the performance of our model on larger and more diverse datasets, integrating additional imaging modalities, implementing 3D visualization of segmented images, exploring real-time detection capabilities, and

applying our model to local datasets. These developments aim to enhance the model's practical applicability and broaden its impact in clinical settings.

Author Contributions: Conceptualization, F.C.; Methodology, F.C., M.M. and S.M.; Software, F.C.; Validation, F.C., M.M. and S.M.; Formal analysis, F.C.; Investigation, M.M. and S.M.; Resources, F.C.; Data curation, F.C.; Writing—original draft, F.C.; Writing—review & editing, F.C., M.M. and S.M.; Visualization, F.C.; Supervision, M.M. and S.M.; Funding acquisition, M.M. and S.M. All authors have read and agreed to the published version of the manuscript.

Funding: This research received no external funding.

Data Availability Statement: Data are contained within the article.

Conflicts of Interest: The authors declare no conflicts of interest.

References

1. Vankdothu, R.; Hameed, M.A. Brain tumor segmentation of MR images using SVM and fuzzy classifier in machine learning. *Meas. Sensors* **2022**, *24*, 100440. [CrossRef]
2. Dang, K.; Vo, T.; Ngo, L.; Ha, H. A deep learning framework integrating MRI image preprocessing methods for brain tumor segmentation and classification. *IBRO Neurosci. Rep.* **2022**, *13*, 523–532. [CrossRef] [PubMed]
3. Jain, D.; Pandey, A.K.; Chauhan, A.S.; Kushwah, J.S.; Saxena, N.; Sharma, R.; Sambrow, V.D.P. ASA-LSTM-based brain tumor segmentation and classification in MRI images. *Int. J. Adv. Technol. Eng. Explor.* **2024**, *11*, 838–851.
4. Taphoorn, M.J.; Klein, M. Cognitive deficits in adult patients with brain tumours. *Lancet Neurol.* **2004**, *3*, 159–168. [CrossRef]
5. Mandle, A.K.; Sahu, S.P.; Gupta, G. Brain tumor segmentation and classification in MRI using clustering and kernel-based SVM. *Biomed. Pharmacol. J.* **2022**, *15*, 699–716. [CrossRef]
6. Agrawal, P.; Katal, N.; Hooda, N. Segmentation and classification of brain tumor using 3D-UNet deep neural networks. *Int. J. Cogn. Comput. Eng.* **2022**, *3*, 199–210. [CrossRef]
7. The Brain Tumour Charity. Brain Tumour Statistics June 2023. 2023. Available online: https://assets.thebraintumourcharity.org/live/uploads/2023/06/Source-K_-Brain-Tumour-Statistics-June-2023-Final-Version.pdf (accessed on 1 August 2024).
8. Ostrom, Q.T.; Gittleman, H.; Fulop, J.; Liu, M.; Blanda, R.; Kromer, C.; Wolinsky, Y.; Kruchko, C.; Barnholtz-Sloan, J.S. CBTRUS statistical report: Primary brain and central nervous system tumors diagnosed in the United States in 2008–2012. *Neuro-Oncology* **2015**, *17*, iv1–iv62. [CrossRef]
9. Solanki, S.; Singh, U.P.; Chouhan, S.S.; Jain, S. Brain tumor detection and classification using intelligence techniques: An overview. *IEEE Access* **2023**, *11*, 12870–12886. [CrossRef]
10. Soltaninejad, M.; Yang, G.; Lambrou, T.; Allinson, N.; Jones, T.L.; Barrick, T.R.; Howe, F.A.; Ye, X. Automated brain tumour detection and segmentation using superpixel-based extremely randomized trees in FLAIR MRI. *Int. J. Comput. Assist. Radiol. Surg.* **2017**, *12*, 183–203. [CrossRef]
11. Ahuja, S.; Panigrahi, B.K.; Gandhi, T.K. Enhanced performance of Dark-Nets for brain tumor classification and segmentation using colormap-based superpixel techniques. *Mach. Learn. Appl.* **2022**, *7*, 100212. [CrossRef]
12. Alwakid, G.; Gouda, W.; Humayun, M.; Jhanjhi, N. Diagnosing melanomas in Dermoscopy images using deep learning. *Diagnostics* **2023**, *13*, 1815. [CrossRef] [PubMed]
13. Khan, A.; Bukhari, J.; Bangash, J.I.; Khan, A.; Imran, M.; Asim, M.; Ishaq, M.; Khan, A. Optimizing connection weights of functional link neural network using APSO algorithm for medical data classification. *J. King Saud-Univ.-Comput. Inf. Sci.* **2022**, *34*, 2551–2561. [CrossRef]
14. Chen, L.C.; Papandreou, G.; Kokkinos, I.; Murphy, K.; Yuille, A.L. Deeplab: Semantic image segmentation with deep convolutional nets, atrous convolution, and fully connected crfs. *IEEE Trans. Pattern Anal. Mach. Intell.* **2017**, *40*, 834–848. [CrossRef] [PubMed]
15. Ronneberger, O.; Fischer, P.; Brox, T. U-net: Convolutional networks for biomedical image segmentation. In Proceedings of the Medical Image Computing and Computer-Assisted Intervention–MICCAI 2015: 18th International Conference, Munich, Germany, 5–9 October 2015; proceedings, part III 18; Springer: Berlin/Heidelberg, Germany, 2015; pp. 234–241.
16. Díaz-Pernas, F.J.; Martínez-Zarzuela, M.; Antón-Rodríguez, M.; González-Ortega, D. A deep learning approach for brain tumor classification and segmentation using a multiscale convolutional neural network. *Healthcare* **2021**, *9*, 153. [CrossRef]
17. Sajid, S.; Hussain, S.; Sarwar, A. Brain tumor detection and segmentation in MR images using deep learning. *Arab. J. Sci. Eng.* **2019**, *44*, 9249–9261. [CrossRef]
18. Farajzadeh, N.; Sadeghzadeh, N.; Hashemzadeh, M. Brain tumor segmentation and classification on MRI via deep hybrid representation learning. *Expert Syst. Appl.* **2023**, *224*, 119963. [CrossRef]

19. Sangeeta, K.; Rahul, M. A Novel Deep Learning Approach for Brain Tumor Segmentation and Classification. *J. Electr. Syst.* **2024**, *20*, 700–710.
20. Pereira, S.; Pinto, A.; Alves, V.; Silva, C.A. Brain tumor segmentation using convolutional neural networks in MRI images. *IEEE Trans. Med. Imaging* **2016**, *35*, 1240–1251. [CrossRef]
21. Ingle, A.; Roja, M.; Sankhe, M.; Patkar, D. Efficient segmentation and classification of the tumor using improved encoder-decoder architecture in brain MRI images. *Int. J. Electr. Comput. Eng. Syst.* **2022**, *13*, 643–651. [CrossRef]
22. Naser, M.A.; Deen, M.J. Brain tumor segmentation and grading of lower-grade glioma using deep learning in MRI images. *Comput. Biol. Med.* **2020**, *121*, 103758. [CrossRef]
23. Sujatha, T.S.; Sreenivasulu, R. U-Net Segmentation for CNN Classification to Improve the Accuracy of Automatic Prediction of Brain Tumors Using MRI Images. *J. Electr. Syst.* **2024**, *20*, 12. [CrossRef]
24. Xu, D.; Zhou, X.; Niu, X.; Wang, J. Automatic segmentation of low-grade glioma in MRI image based on UNet++ model. In Proceedings of the 2020 3rd International Conference on Computer Information Science and Artificial Intelligence (CISAI) 2020, Inner Mongolia, China, 25–27 September 2020; p. 7.
25. Bedi, P.; Ningshen, N.; Rani, S.; Gole, P.; Bhasin, V. CT-γ-Net: A Hybrid Model Based on Convolutional Encoder-Decoder and Transformer Encoder for Brain Tumor Localization. *J. Data Sci. Intell. Syst.* **2024**, *15*. [CrossRef]
26. Kunjumon, A.; Jacob, C.; Resmi, R. An Efficient U-Net based Model for Low Grade Glioma Segmentation in MRI Images. In Proceedings of the 2024 Second International Conference on Emerging Trends in Information Technology and Engineering (ICETITE), Vellore, India, 22–23 February 2024; pp. 1–5.
27. Chahbar, F.; Merati, M.; Mahmoudi, S.; Baghdadi, M.; Lebani, Z.A. Brain Tumor Classification in Magnetic Resonance Imaging using Convolutional Neural Networks and Transfer Learning. In Proceedings of the IAM 2023: The 6th International Hybrid Conference on Informatics and Applied Mathematics, Guelma, Algeria, 6–7 December 2023; Volume 6.
28. Ibtehaz, N.; Rahman, M.S. MultiResUNet: Rethinking the U-Net architecture for multimodal biomedical image segmentation. *Neural Netw.* **2020**, *121*, 74–87. [CrossRef]
29. Yu, F. Multi-scale context aggregation by dilated convolutions. *arXiv* **2015**, arXiv:1511.07122.
30. Chen, L.C.; Zhu, Y.; Papandreou, G.; Schroff, F.; Adam, H. Encoder-decoder with atrous separable convolution for semantic image segmentation. In Proceedings of the European Conference on Computer Vision (ECCV), Munich, Germany, 8–14 September 2018; pp. 801–818.
31. Li, X.; Chen, H.; Qi, X.; Dou, Q.; Fu, C.W.; Heng, P.A. H-DenseUNet: Hybrid densely connected UNet for liver and tumor segmentation from CT volumes. *IEEE Trans. Med. Imaging* **2018**, *37*, 2663–2674. [CrossRef]
32. Al-Dhabyani, W.; Gomaa, M.; Khaled, H.; Aly, F. Deep learning approaches for data augmentation and classification of breast masses using ultrasound images. *Int. J. Adv. Comput. Sci. Appl.* **2019**, *10*, 1–11. [CrossRef]
33. Yang, M.; Yu, K.; Zhang, C.; Li, Z.; Yang, K. Denseaspp for semantic segmentation in street scenes. In Proceedings of the IEEE Conference on Computer Vision and Pattern Recognition, Salt Lake City, UT, USA, 18–23 June 2018; pp. 3684–3692.
34. Buda, M.; Saha, A.; Mazurowski, M.A. LGG Segmentation Dataset. 2019. Available online: https://www.kaggle.com/datasets/mateuszbuda/lgg-mri-segmentation (accessed on 18 April 2024).